LUND UNIVERSITY

Simultaneous multispectral imaging of flame species using Frequency Recognition Algorithm for Multiple Exposures (FRAME)

Li, Zheming; Borggren, Jesper; Berrocal, Edouard; Ehn, Andreas; Aldén, Marcus; Richter, Mattias; Kristensson, Elias

Simultaneous multispectral imaging of flame species using Frequency Recognition Algorithm for Multiple Exposures (FRAME)

Zheming Li[a], Jesper Borggren[a], Edouard Berrocal[a,b], Andreas Ehn[a], Marcus Aldén[a], Mattias Richter[a], Elias Kristensson[a,*]

[a] *Division of Combustion Physics, Lund University, Lund, Sweden*
[b] *Erlangen Graduate School in Advanced Optical Technologies (SAOT), Universität Erlangen-Nürnberg, Erlangen, Germany*

ABSTRACT

Imaging the interaction between different combustion species under turbulent flame conditions requires methods that both are extremely fast and provide means to spectrally separate different signals. Current experimental solutions to achieve this often rely on using several cameras that are time-gated and/or equipped with different spectral filters. In this work we explore a technique called Frequency Recognition Algorithm for Multiple Exposures (FRAME) as an alternative solution for instantaneous multispectral imaging of flame species. The method is based on exciting different species with different spatial "codes" and to separate each signal component using a spatial frequency-sensitive lock-in algorithm. This methodology permits the signal from several different species to be recorded at the exact same time with a single camera. Furthermore, since the signals are recognized based on the superimposed spatial codes, there is no need for spectral separation prior to detection. The entire fluorescence envelope from each species can thus, in principle, be detected. In the current work, we present simultaneous planar laser-induced fluorescence imaging of OH and CH_2O in a turbulent dimethyl ether (DME)/air flame.

© 2018 The Authors. Published by Elsevier Inc. on behalf of The Combustion Institute.
This is an open access article under the CC BY license. (http://creativecommons.org/licenses/by/4.0/)

1. Introduction

Most combustion phenomena are three-dimensional (3D) processes that involve complex multi-species chemical interactions, turbulent mixing with rapid structural changes, high temperature gradients and sometimes multi-phase fluid dynamics [1,2]. All these characteristics make it technically challenging to investigate the process, and, at present, no single diagnostic tool can provide sufficient data to fully describe these complex systems. Tomographic imaging opens up for 3D imaging but is practically limited to chemiluminescence imaging [3,4] or laser-probing of one specific combustion species [5]. Transmission laser-based imaging can provide information about phase-transitions and/or temperature gradients [6], but the data is line-of-sight integrated, limiting what conclusions can be drawn from the data. Laser sheet imaging is commonly used for combustion research as a "workaround" of the problems associated with the sample's three-dimensionality [7]. With this technique, the sample is irradiated with a thin sheet of light – often using a pulsed laser – and the signal is collected at a 90° angle. One of many benefits with laser sheet imaging is its versatility; planar Rayleigh scattering may provide tempera-

ture mapping [8,9], planar laser-induced fluorescence (PLIF) imaging can give species concentration [10], laser-induced incandescence yields the soot volume fraction [11], velocity fields can be deduced using Particle Imaging Velocimetry [12], to name a few examples. Laser sheet imaging can also be used to study interactions between key combustion species by simultaneously recording the spatial distribution of different species, which is especially important for correlation studies of species that overlap in space [13–22]. However, experimental approaches for "simultaneous" detection of several combustion species often rely on sequential detection using several time-gated cameras, often in combination with spectral filters/mirrors that separate the emitted signal onto the different cameras (or regions on the sensor) [13–22]. While the use of several cameras can be advantageous in some situations e.g. for detection of significantly different wavelengths where a combination of cameras having different characteristics/sensitivities facilitates the experiment, the methodology has certain drawbacks; (1) systems based on several intensified cameras are expensive and, sometimes, impractical, (2) different species that have spectrally overlapping emissions can be challenging to probe due to the risk of signal cross-talk and (3) procedures to compensate for differences in the collection optics and camera efficiencies as well as post-processing means to achieve an accurate pixel-to-pixel correspondence are often required.

* Corresponding author.
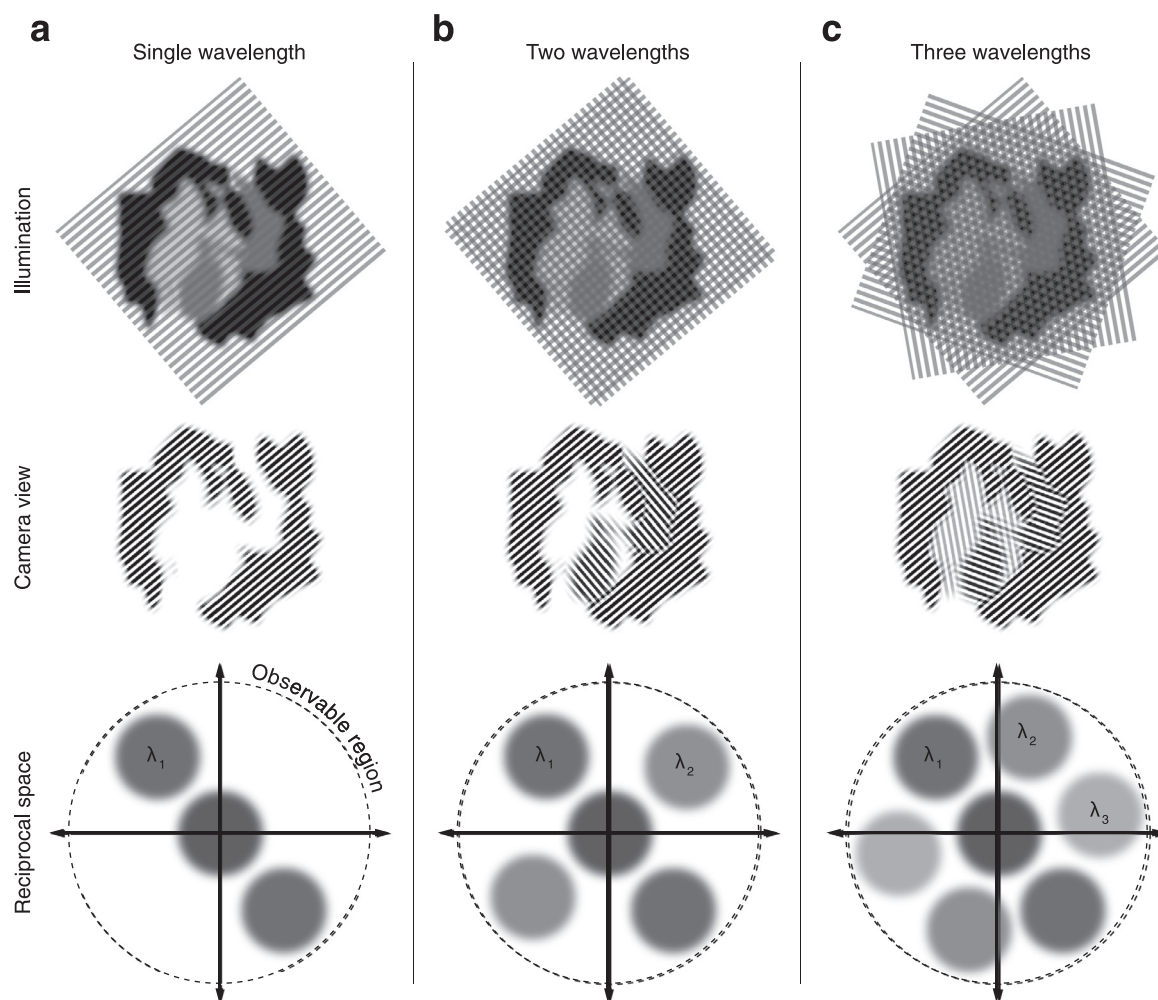 *E-mail address:* elias.kristensson@forbrf.lth.se (E. Kristensson).

Fig. 1. A conceptual illustration of the FRAME principle. A sample with three different constituents is illuminated with differently coded light fields. (a) A single modulated laser-probe illuminate the sample, creating two "copies" of the sample structures of one constituent at $\pm v$. (b, c) By illuminating the sample with differently coded laser-probes, it is possible to transfer data from the different constituents into different regions in reciprocal space.

In this paper, we explore an alternative method to tackle the problem associated with multispectral data acquisitions. The method, which is referred to as Frequency Recognition Algorithm for Multiple Exposures (FRAME) in the literature [23,24], employs a coded laser-probe illumination strategy to distinguish between different signal components. Dorozynska and Kristensson recently demonstrated how this coding strategy could be exploited in order to acquire multispectral 2D information instantaneously [25]. In the current study, we continue exploring the potential of the FRAME technique for simultaneous multispectral imaging, primarily seeking to investigate the merits of FRAME for gas-phase, combustion diagnostics. To reach sufficient signal-to-noise (SNR) levels we transfer the wide-field FRAME imaging concept adopted by Dorozynska and Kristensson into a laser sheet arrangement. With this setup we here demonstrate, for the first time, the ability to perform simultaneous multispectral PLIF imaging of combustion species – OH and CH_2O – with a single camera by means of FRAME.

2. Frequency Recognition Algorithm for Multiple Exposures (FRAME)

FRAME is an imaging technique that allows a mono-camera setup to record several laser-probe images in one single acquisition [23–25]. Under normal circumstances such an approach would

yield an image wherein all the different 2D signal components would be irreversibly mixed. Separating the different images would require knowledge about the spatial distribution and the concentration of the sample constituents – the quantities one seeks to determine. FRAME solves this "problem" by employing a coded illumination strategy, where each individual fluorescence image becomes encoded with a specific periodic line structure (pure sinusoidal or top-hat). The illumination scheme is similar to that used for Structured Illumination Planar Imaging (SLIPI) [26–28] but unlike SLIPI, FRAME accesses all data from a single recording, albeit at the cost of a reduced spatial resolution. The 2D signal from each laser-probe can thus be distinguished and separated from each other in the data post-processing by means of a frequency-sensitive spatial lock-in algorithm [29,30]. Here we will first describe the FRAME principle conceptually followed by a mathematical description of the method and the lock-in algorithm.

In the conceptual example presented in Fig. 1, a sample with three different constituents is illuminated using the coded illumination approach. In Fig. 1a, the sample is illuminated with a single modulated (frequency v_1) laser-probe at a wavelength of λ_1, sensing the spatial distribution of one constituent. The sample structures and laser light are superposed multiplicatively, effectively creating three "copies" of the sample structures in reciprocal space (Fourier domain), one in the origin and two centered at $\pm v_1$. If the modulation frequency is sufficiently high, the "copies" will be
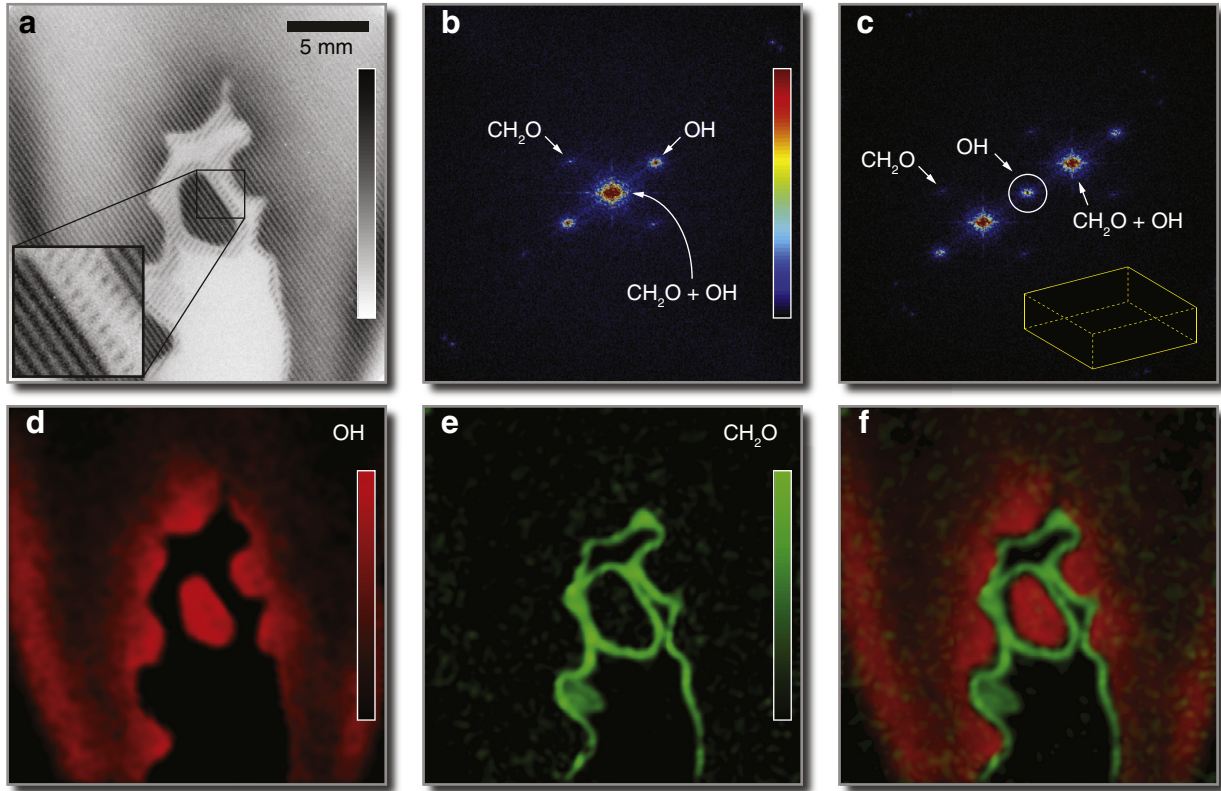
Fig. 2. The spatial lock-in algorithm. (a) Unprocessed image containing fluorescence signals from both OH and CH_2O. The magnified region highlights the difference in modulation between the two signal components. (b) The Fourier transform of (a) wherein the different image components are indicated. (c) The Fourier transform of the raw data after multiplication with the OH modulation frequency. Also included here is the low-pass filter function (circle marks its position). (d) OH image extracted from (a). (e) CH_2O image extracted from (a). (f) Multispectral image of both combustion species. Note that all images have been histogram-adjusted. A filter size of $\sigma = 0.17$ (see Section 4.3) has been used for the extraction of (d)–(f).

isolated from each other, as illustrated in Fig. 1a. In Fig. 1b and c differently coded laser sources excite the remaining constituents of the sample *simultaneously*, thus transferring "copies" of the different sample structures into different, isolated regions in reciprocal space. The acquired image – containing data from all constituents – is then analyzed with an algorithm that only extracts information that is modulated with a certain spatial frequency.

To explain the FRAME principle and lock-in algorithm mathematically, consider the case given in Fig. 1b, where a sample is illuminated with two differently coded laser-probes. The signal recorded by the camera can be expressed as follows:

$$I(x, y) = S_1(x,y)\big(1 + \sin\big(2\pi\nu_{1,x}x + 2\pi\nu_{1,y}y\big)\big)$$
$$+ S_2(x,y)\big(1 + \sin\big(2\pi\nu_{2,x}x + 2\pi\nu_{2,y}y\big)\big) \tag{1}$$

where $I(x, y)$ is the acquired image, S_1 and S_2 are the two sample responses and ν are spatial frequencies (the spatial phase of the modulation is omitted for reasons of clarity). From this data we now aim to extract the sample responses individually, here derived for the extraction of S_1. Multiplying Eq. (1) with a sine wave having the modulation frequency $\bar{\nu} = \nu_{1,x} + \nu_{1,y}$ yields:

$$I(x, y) \sin\big(k\nu_{1,x}x + k\nu_{1,y}y\big) = \frac{1}{2}\Big(S_2 \cos\big(k(\nu_{1,x} - \nu_{2,x})x$$
$$+ 2\pi\big(\nu_{1,y} - \nu_{2,y}\big)y\big) - S_2 \cos\big(k(\nu_{1,x} + \nu_{2,x})x + k\big(\nu_{1,y} + \nu_{2,y}\big)y\big)$$
$$+ 2S_1 \sin\big(k\nu_{1,x}x + k\nu_{1,y}y\big) - S_1 \cos\big(2k\nu_{1,x}x + 2k\nu_{1,y}y\big)$$
$$+ 2S_2 \sin\big(k\nu_{1,x}x + k\nu_{1,y}y\big) + S_1\Big) \tag{2}$$

Frequency analysis of Eq. (2) (where $k = 2\pi$) reveals several different frequency components, yet only a single DC component – the last S_1 term. Thus, by applying a low-pass filter with a cut-off frequency ν_c, where $\nu_c < \nu_{1,x} + \nu_{1,y}$ and $\nu_c < \nu_{2,x} + \nu_{2,y}$, all terms but the S_1 term are rejected, thus revealing the sample structures of S_1. The second sample constituent, S_2, is then accessed in a similar fashion, i.e. by multiplying Eq. (1) with a sine wave having the modulation frequency $\bar{\nu} = \nu_{2,x} + \nu_{2,y}$. It should be noted that to avoid ambiguities caused by the spatial phases, which were omitted in the derivation, Eq. (1) also needs to be multiplied with $\cos(k\nu_{1,x}x + k\nu_{1,y}y)$. Combining both expressions cancels out the spatial phase, see also Refs. [29,30] for more detailed derivations of the spatial lock-in algorithm (albeit in one dimension only).

Figure 2 illustrates the mathematical procedure of the lock-in algorithm graphically. Figure 2a shows an unprocessed image containing planar laser-induced fluorescence signals from both OH and CH_2O, generated using the FRAME setup used in the current study. The Fourier transform of Fig. 2a (Fig. 2b) reveals the two image components stored simultaneously on chip. Multiplying the input image with a 2D sine wave that exactly matches the modulation frequency of the OH signal effectively demodulates the fluorescence from OH (Fig. 2c), i.e. the complex information is shifted so that the modulation frequency of OH is placed at the origin. The rearranged dataset is then filtered using a low-pass Gaussian filter (see inset), thus extracting the OH image and removing the information arising from CH_2O. Calculating the inverse Fourier transform turns spatial frequencies into intensity values, revealing the OH distribution (Fig. 2d). The procedure is then repeated for the fluorescence signal emitted by the CH_2O molecule (Fig. 2e). In
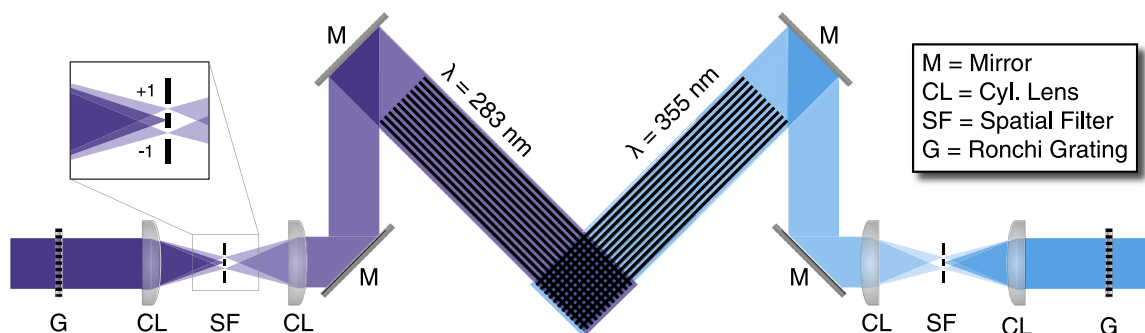
Fig. 3. FRAME experimental setup. Two identical optical arrangements were created for the laser excitation sources. In the setup, a transmission grating was illuminated and a cylindrical lens was used to form an image of the grating. A spatial filter, placed in the Fourier plane of the first cylindrical lens, rejected all but the ±1 diffraction orders of the grating in order to create a pure sinusoidal intensity modulation (by interference). A second cylindrical lens was then used to compress the light field into a thin sheet. Two mirrors were used to alter the angle of incidence, to transfer the fluorescence signal from each laser sheet into different regions in the Fourier domain of the acquired image. An ICCD camera (Princeton PI-MAX4) recorded the fluorescence emitted at 90°.
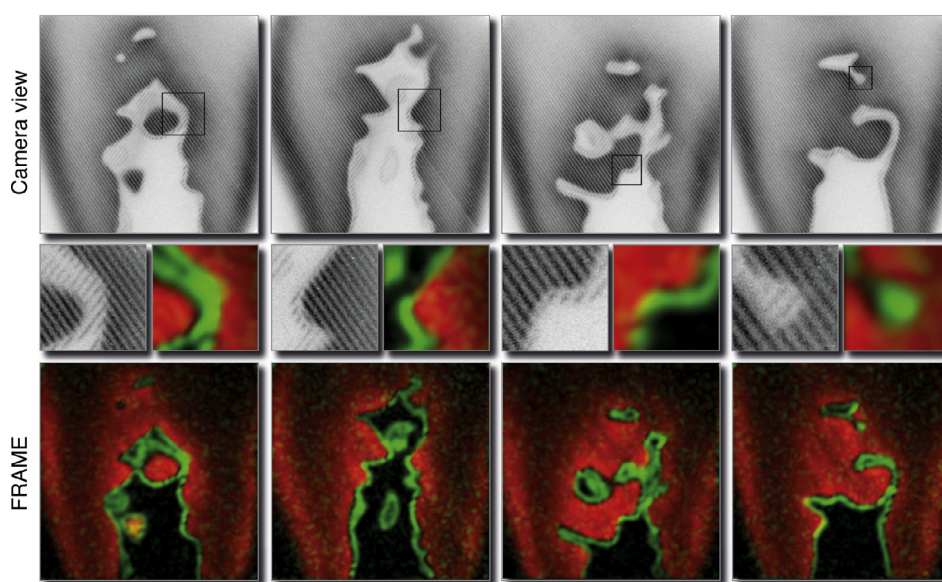

Fig. 4. Simultaneously acquired multispectral images of OH and CH_2O in a Bunsen flame. (Top row) Four unprocessed images, as seen by the camera, recorded using the FRAME setup. (Bottom row) Multispectral information after analyzing each image with the lock-in algorithm (filter size $\sigma = 0.17$).

Fig. 2f the two images are false colored and merged into a multispectral image.

3. Experimental setup

Figure 3 shows a schematic of the optical arrangement used in the experiment. A frequency-tripled Nd:YAG laser ($\lambda = 355$ nm, pulse energy ≈ 100 mJ) was used to excite the formaldehyde molecules, while the hydroxyl molecules were stimulated using a frequency doubled dye laser ($\lambda = 283$ nm, pulse energy ≈ 10 mJ), pumped by a pulsed Nd:YAG laser ($\lambda = 532$ nm). The optical arrangements were identical for the two different light sources. After being expanded and collimated, the beams were each guided through a Ronchi grating (10 lp/mm), diffracting the beams into several different diffraction orders. To form the sinusoidal line pattern in each beam path, a cylindrical lens ($f = 150$ mm) was used in conjunction with a spatial filter, which only permitted the ±1 orders of diffraction. Employing a spatial filter is not strictly required – the grating can be imaged directly onto the measurement region – but it does simplify the alignment procedure since the exact distance between the cylindrical lens and the sample becomes less crucial (the two orders create the intensity modula-

tion by interference). One drawback with this approach is the reduction of the laser energy, where $\sim$50% is lost due to reflection upon the Ronchi grating and thereafter $\sim$70% of the remaining energy is blocked by the spatial filter. Although the final photon flux was sufficient for the current proof-of-concept investigation, applications with low SNR conditions may require alternative optical configurations where the laser power is better preserved. Kristensson et al. employed a structured illumination scheme based on a double-wedged glass plate, which yields insignificant losses in photon flux [31]. Another potential solution would be to create the intensity modulation by means of a phase grating – a transparent optical component that diffracts the transmitted light directly into the desired ±1 orders. Employing such lossless structured illumination schemes thus have the potential of improving the photon flux by a factor of $\sim$6, although this needs to be confirmed through experimental work.

A second cylindrical lens ($f = 1000$ mm) was then used to compress each laser beam into a thin sheet of light ($\sim$200 μm thickness). Maximizing the modulation depth for each beam path requires fine-tuning of the orientation of the grating as well as both cylindrical lenses. Real-time monitoring of the Fourier transform of the acquired image can thus facilitate in this procedure. Finally,
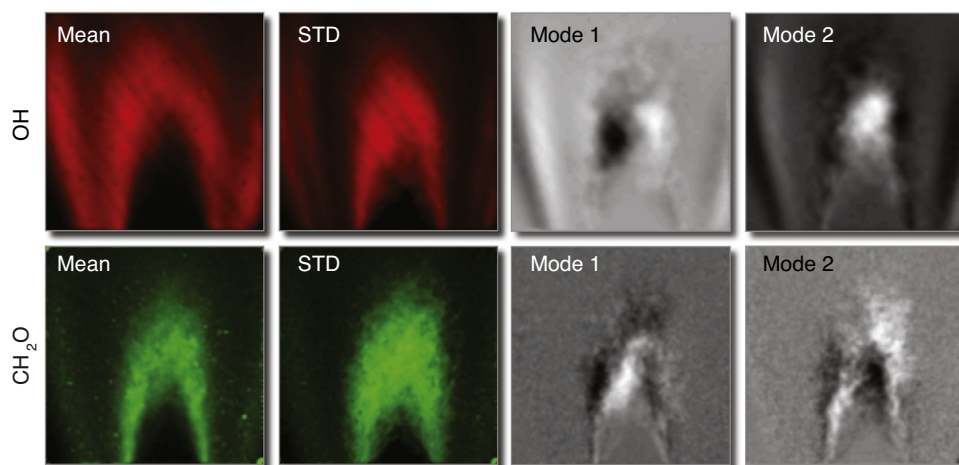
Fig. 5. Statistical analysis of the acquired dataset (200 snapshots) for both OH and CH$_2$O. The figure shows mean fields, standard deviations and the two most dominant modes from POD analysis for both combustion species.

two mirrors were used in both beam paths to guide the laser sheets onto the sample from different angles in order to transfer the corresponding fluorescence into different regions in the Fourier domain. An intensified CCD (ICCD) with a pixel resolution of 1024 × 1024, positioned at a 90° angle configuration, was used to image the fluorescence from the two species simultaneously using a Halle lens (focal length = 100 mm, $f_\# = 2$). A 290 nm long-pass filter and 355 nm notch filter were applied to remove the scattering signals. The burner was a Bunsen type burner, providing a premixed, slightly fuel rich DME/air flame.

4. Results and discussion

4.1. Multispectral imaging results

Figure 4 shows four examples of multispectral images, acquired simultaneously using the planar FRAME setup. The top row in Fig. 4 shows the raw data, as seen by the camera. The magnified regions highlight how the signal from OH and CH$_2$O differs in terms of their modulated structure, making it possible to, even by eye, distinguish the signal from the two species. Each set of data is then analyzed using the FRAME algorithm, which separates the species, the result of which is shown in the bottom row (false coloring). Note that no correction for e.g. flat-field compensation or background suppression has been applied to the data. Since the data are not quantitative, the signal from each species is histogram-adjusted and normalized to unity in the presented data. The data show that the formaldehyde is formed in the area where the pre-heat zone and the reaction zone meet whereas the OH molecule is present in the product zone, which is in agreement with past knowledge [13,15,32–34]. The formaldehyde visible in the high temperature regions is due to the relatively low SNR for the formaldehyde signal, which, as mentioned above, is primarily due to the losses caused by the approach currently used to generate the line structures. The use of e.g. phase gratings or double-wedged glass plates should increase the SNR for improved sensitivity.

Figure 5 presents statistical analysis performed on the acquired dataset (200 snapshots), showing averaged images, standard deviations in 2D and mode analysis (two most dominant modes). Mode analysis (or Proper Orthogonal Decomposition, POD) is an analytical tool to statistically investigate a dynamic behavior (in particular oscillatory modes) and is based on decomposing an ensemble of images (or 1D arrays) into a set of Eigen functions (modes). The modes represent fluctuations from the mean field, where any

snapshot in the dataset can be reconstructed using a linear combination of the modes. For more details on the theory of POD and its applications for combustion studies, see Refs. [35–38].

In 1998, Paul and Najm proposed that taking the pixel-by-pixel product of OH and CH$_2$O images yields an image that displays the reaction rate [33]. The ability to collect both these data simultaneously as well as an accurate pixel-by-pixel correlation is thus key for such data analysis. Figure 6 shows four typical FRAME measurements using the current setup, from which this product is calculated. Since both images are acquired using the exact same collection optics and camera system, corrections procedures to reduce measurement uncertainties associated with these parameters are not needed. Note that the relatively low SNR of the CH$_2$O leads to both the non-zero values of reaction rate in the high temperature regions as well as the zero values of heat release in the reaction zone.

4.2. Spectral filtering

The ability to access multispectral information simultaneously with a single detector also opens up for new measurement possibilities for e.g. spectral filtering and suppression of interferences. For example, detecting species having fluorescence signals that partly or entirely overlap spectrally is technically challenging with multispectral imaging schemes that rely on spectral filters. Examples of combinations of combustion species whose fluorescence signals are difficult to separate spectrally are (1) acetone, CH and CH$_2$O [39–45] and (2) OH and toluene [41,46–48]. Using several time-gated cameras to acquire the signals sequentially solves the problem, but it is an expensive solution. Since FRAME uses spatial codes to distinguish between signal components, it could, in principle, be used to detect and separate species with similar – or even identical – spectral emission characteristics. Note that notch filters may still be required to prevent detection of laser scattering. A further potential advantage of avoiding spectral filters to separate signal components by means of FRAME is an improved SNR, since it may allow detection of the entire fluorescence envelope rather than only selecting (spectrally) the non-overlapping part. Of course, this would require a more light-efficient FRAME setup, as those mentioned in the Experimental setup section, so that the lower excitation flux does not negate the improved emission collection.

Another potential benefit with FRAME concerns the detection and suppression of interfering signal components arising from broadband absorbers and/or stray light generated by e.g.
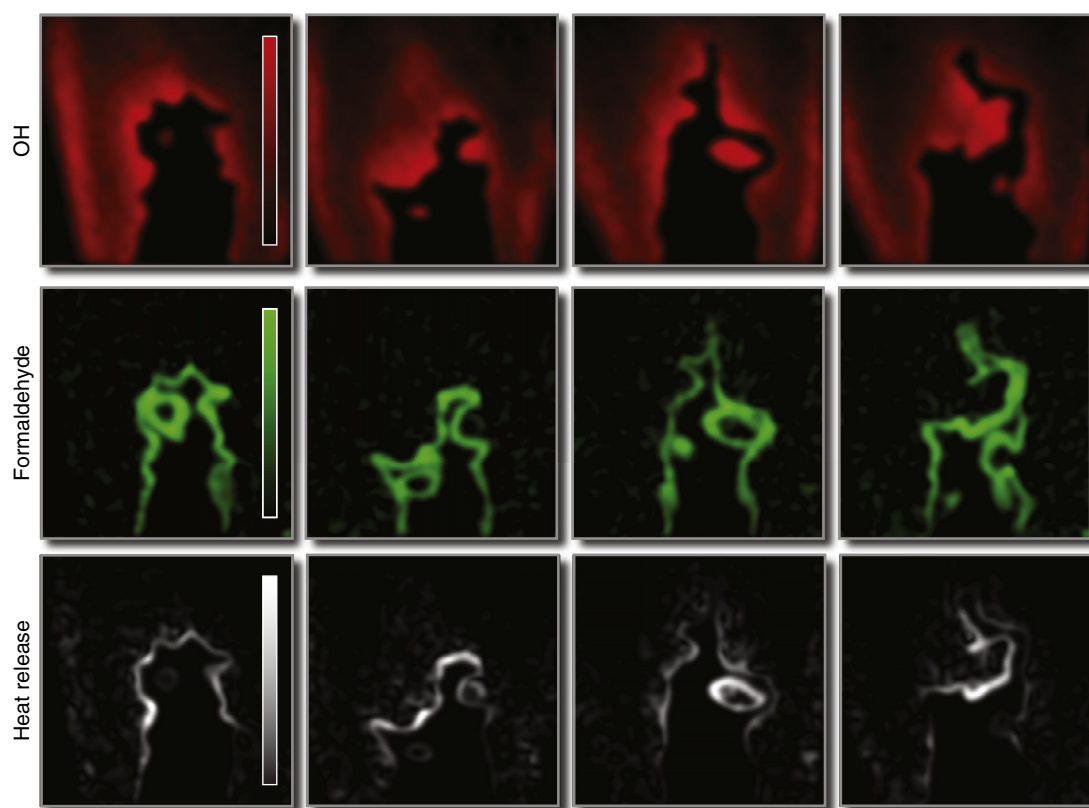
Fig. 6. Pixel-by-pixel product of OH and CH$_2$O images. Taking the product of the OH (top row) and the CH$_2$O (middle row) images yields intensity maps that are closely related to the reaction rate (bottom row) [15,33].

reflections. Reducing the undesired non-resonant emission from broadband absorbers is commonly accomplished by performing two measurements; one where the laser source is tuned on the resonance line and then one off resonance, where the latter functions as a background measurement [49,50]. With FRAME, both these measurements could, in principle, be acquired simultaneously. Measurements based on Rayleigh scattering as well as resonance fluorescence detection are often subject to stray light contamination, caused by e.g. laser reflections on the windows in the optical ports. This problem, which cannot be addressed using optical filters, is usually addressed by (1) painting the interior of the combustion chamber black, (2) measuring the stray light when the laser is tuned off resonance and/or (3) assessing the stray light level without the flame ignited. However, as demonstrated by Kristensson et al. [31], stray light will not carry the information encoded into the laser sheets and will therefore also be suppressed in the FRAME data post-processing.

4.3. Spatial resolution

The ability to store several images simultaneously on the camera sensor comes at the price of a reduced spatial resolution per extracted image. For traditional photography, the spatial resolution achievable depends mainly on (1) the number of pixels of the detector and (2) the modulation transfer function (MTF) of the imaging system, i.e. the optical properties. However, laser sheet imaging in general, and planar laser-induced fluorescence imaging of gaseous samples in particular, has one more factor that influences the spatial resolution – the thickness of the laser sheet. This can be understood by considering that the sample extends in 3D and that the laser sheet is generating a signal in the entire volume it is encountering. Although, it is also important to realize that not

all objects carry structural details finer than those resolvable by a given imaging system. In these cases, the data is over-sampled.

The spatial resolution of images extracted from a FRAME measurement depends on two additional factors; the spatial frequency of the superimposed intensity modulation and the low-pass filter used in the spatial lock-in algorithm. These two parameters are closely linked. Increasing the size of the low-pass filter means including more spatial frequencies, which yields an improved spatial resolution. However, the size of the filter cannot exceed a certain limit, after which cross-talk between neighboring images (in reciprocal space) becomes apparent (see example in Fig. 7). Generally, the more isolated each image copy is in the Fourier domain, the better the end resolution becomes. It is therefore advisable to maximally disperse the image copies in reciprocal space and use the highest intensity modulation frequency resolvable by the imaging system. Unfortunately, intensified (multi-channel plate, MCP) cameras tend to have an MTF that rolls off relatively fast, which is because fine structural details are lost in the conversion from photons to electrons and then back to photons again. This characteristic becomes a limiting factor when employing the FRAME concept with intensified cameras, because the intensity modulation frequency must be kept relatively low (to be kept within the borders of the MTF). Consequently, this affects the settings of the low-pass filter whose dimensions also become relatively small.

Figure 7 illustrates how the spatial resolution of the extracted images is influenced by the settings of the low-pass filter. The example shows a raw, unprocessed image that contains both OH and CH$_2$O data together with its Fourier transformation after the OH image copy has been demodulated (compare with Fig. 2c). The OH image is then extracted using five differently sized filters, where the σ-value in each frame indicates the integrated area of the low-pass filter (acceptance of spatial frequencies) given as a percentage
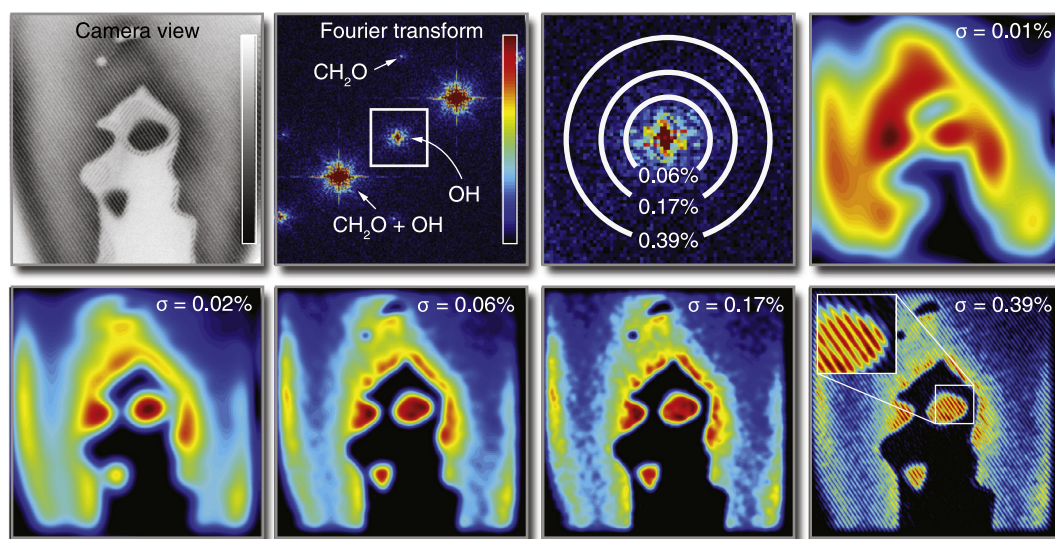
Fig. 7. FRAME data extracted using differently sized filters. The example shows that a too narrow filter function generates images with poor spatial resolution, while a too wide filter can lead to signal cross-talk. The analysis thus reveals suitable intermediate values of the filter size (σ).
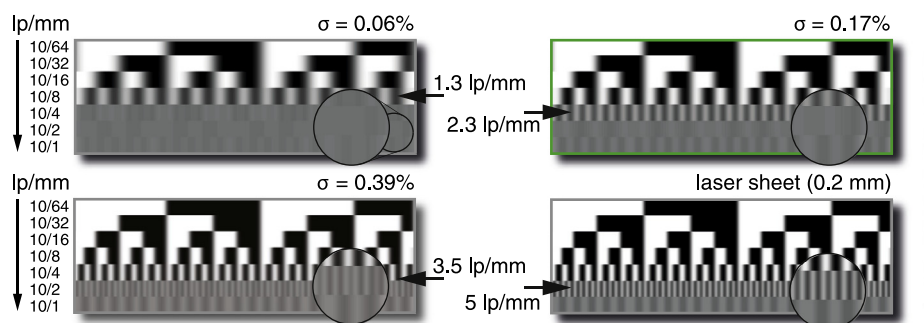

Fig. 8. The effect on spatial resolution for differently sized filter kernels. In the analysis, different low-pass filters are applied on the synthetic image (1024×1024 pixels) of a binary resolution target to give an idea of the spatial resolution achievable for certain experimental constraints (indicated by the specified numbers and corresponding arrows). Also shown is an estimate of the spatial resolution achievable with a 200 μm thick laser sheet.

of the area of the Fourier domain. A filter that covers the entire reciprocal space has a σ-value of 100%. At low values of the filter, most image details are lost. Although, already at 0.06% the OH distribution starts to become apparent. When the filter is increased beyond a certain limit information from neighboring images (or the 0th order) fall within the filter and creates an interfering signal. The last example in Fig. 7 ($\sigma = 0.39\%$) shows such interference, which is manifested as lines. Note that in this particular example, the cross-talk comes from the 0th order data (originally contained in the origin) and not the neighboring CH_2O image copy.

The FRAME concept relies on the fact that the power spectrum of an image is strongly shifted towards the low spatial frequencies [51]. To further illustrate this fact, we present a set of synthetic images of a resolution target that have been processes with different filter settings (Fig. 8). The figure shows results from three of the filters in Fig. 7 where, as before, σ indicates the integrated area of the low-pass filter divided by the full area of the sensor, given in percentage. Also included in Fig. 8 is an image of the resolution target that shows the spatial resolution achievable with a 200 μm thick laser sheet setup. Note that the calculations are based on a detection system that has a pixel resolution of 1024×1024 and that FRAME would benefit, both in terms of image-storing capabilities as well as the spatial resolution, of having a higher number of pixels (as is true for nearly all types of imaging measurements). This type of analysis can act as guidance, making it possible to determine how a FRAME setup should be ar-

ranged depending on what structures one desires to observe. In the current experiment and with the current imaging conditions, the maximum size of the low-pass filter was 0.17%, which gives a spatial resolution of ~0.4 mm (2.3 lp/mm), i.e. corresponding to the resolution achievable with a 0.4 mm thick laser sheet. This spatial resolution was deemed sufficient for this proof-of-concept demonstration of FRAME, allowing observation of the spatial distribution of both the OH- and CH_2O molecules on a macroscopic scale. However, more detailed studies of e.g. the overlap between different combustion species using FRAME would require an improved spatial resolution to avoid ambiguities caused by spatial broadening. Observing finer details with FRAME can be accomplished in two ways. First, by increasing the intensity modulation frequency a larger low-pass filter can be used in the FRAME image extraction process. For example, increasing this frequency by a factor of ~1.5 would permit the use of ~6 times larger filter. This calculation illustrates an important feature; the relationship between filter size and modulation frequency is not linear and a relatively small increase in modulation frequency can yield a significant improvement in spatial resolution. Second, reducing the field-of-view (currently ~25×25 mm) through optical magnification also improves the spatial resolution, given that the modulation frequency is increased accordingly (achieved by e.g. down-collimating the excitation sheets).

Figure 9 illustrates the relationship between modulation frequency and filter size on a set of synthetically generated images.
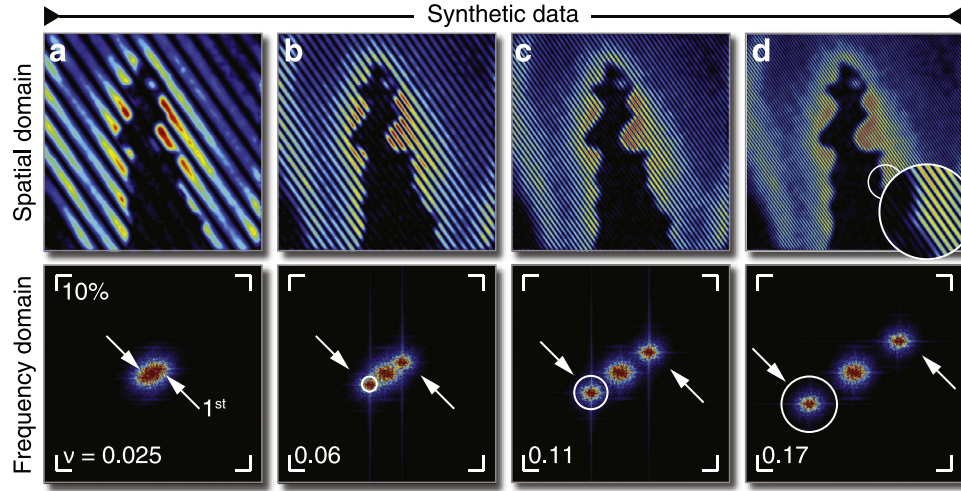
Fig. 9. Illustration on the importance of modulation frequency (synthetic data). Four examples of an OH image acquired with different modulation frequencies. At very low spatial frequencies, (a), the ±1 orders (arrows) overlap significantly with the 0th order in reciprocal space (bottom row), making it difficult to extract the intensity modulated information without cross-talk. However, when the modulation frequency is sufficiently high, cases (c) and (d), the OH information becomes isolated in reciprocal space. The normalized modulation frequency for each case is given in the corresponding Fourier transformation.
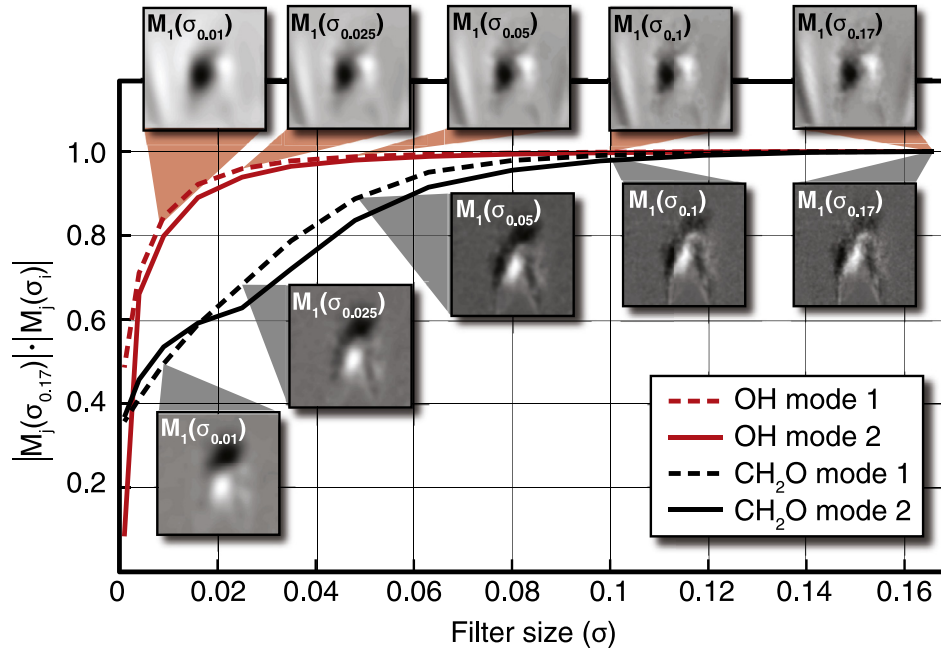

Fig. 10. Investigation on how sensitive mode analysis is to the filter size (σ) used in the FRAME image extraction procedure. The OH and CH_2O datasets (from 200 acquisitions) were extracted using 13 different filter sizes (σ). POD analysis was then performed on each of these 13 sets of single-shot FRAME data to produce 13 sets of Eigen modes. In this analysis, merely the two most dominant Eigen modes were considered and the modes that were extracted from the dataset with the highest spatial resolution ($\sigma = 0.17$) were used as a reference case. This comparison was made by calculating the scalar product between the reference modes and their equivalence from datasets with lower spatial resolution. Values near unity should be interpreted as though no image information has been lost when computing the modes from FRAME images that have been extracted with a reduced filter size.

A very low modulation frequency, case (a), leads to a condition where the coded information cannot be accessed due to a too large overlap with the low frequency data. As the modulation frequency is increased the overlap between structures in the reciprocal space reduces, which allows access to the frequency-shifted data. Notice how a higher modulation frequency yields conditions that permit larger filters without introducing cross-talk with lower spatial frequencies (circles in Fig. 9).

The spatial resolution required for drawing conclusions based on visual observations or statistic analysis is highly case-dependent. Mode analysis (POD), which uses a large dataset to extract Eigen functions (or spatial modes), is an powerful analytical tool that FRAME imaging potentially is well-suited for since it requires snapshot data. To investigate how sensitive POD is to spatial resolution, the acquired dataset of 200 snapshot images were analyzed using the FRAME algorithm with 13 different filter sizes (σ) for both the OH and CH_2O signals. Mode analysis was then performed on all 13 datasets for both combustion species, and the two most dominant modes for each individual case were extracted. To determine how the spatial resolution of the images that are extracted by the FRAME algorithm is affecting the set of Eigen modes, each set of 13 modes was compared with its corresponding reference case. The reference case was extracted using a filter size of $\sigma = 0.17$ which was the largest filter size used in this current
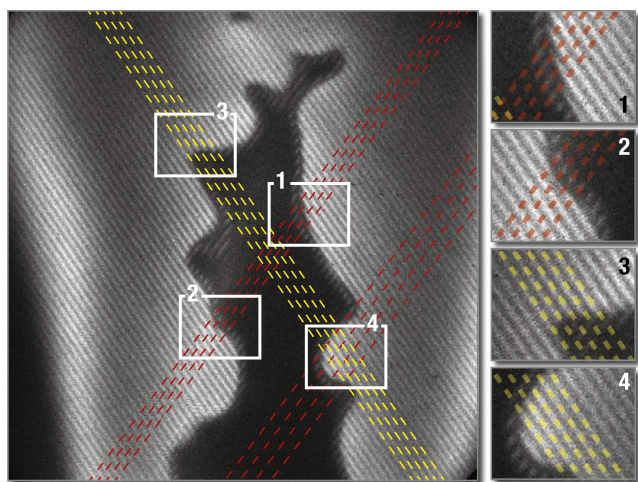
Fig. 11. Investigation on whether beam steering is visually apparent in the data. The figure shows one unprocessed recording of both OH and CH_2O, wherein a set of parallel lines has been drawn, fitted to trace the line structure for each modulated excitation pulse. No signs of beam steering – that potentially could redirect the lines – are observed when tracing the line structures across the unburned region between the two reaction zones, as seen in the four regions-of-interest.

analysis (see also Fig. 7). The comparison between the two most dominant modes in the reference case (denoted $M_j(\sigma_{0.17})$ in Fig. 10, where $j =$ mode number) and the remaining 12 sets of mode images was based on computing their scalar product, giving values between zero and unity. A value of one means that the mode analysis is unaffected by the reduction of the filter size, and thus the same modes can represent both image sets. If, however, the scalar product is zero there is no correlation between the mode image and its reference case (image vectors are orthogonal). The results from this investigation are displayed in Fig. 10. A filter size, σ, above ~ 0.12 yields virtually no effect (scalar product of ≥ 0.99) on the POD analysis on the set of CH_2O data, whereas the equivalent number for the set of OH data is $\sigma \approx 0.06$. In practice, this means that the same set of Eigen modes can be used to represent OH and CH_2O data if the filter size is kept above these numbers. However, the Eigen-mode analysis starts to be affected if smaller filter widths are used. Although the results are slightly different for OH and formaldehyde – which we attribute to differences in their spatial distribution – the results show that the loss in image resolution caused by FRAME does not have a significant impact on mode analysis.

4.4. Beam steering

Refraction occurring due to a sudden change in refractive index – beam steering – is a potential concern for FRAME imaging since the method is based on extracting light that carries a specific periodic line structure. Significant beam steering occurring in the flame will thus distort the periodic pattern, which would lead to a reduced signal level. For laser sheet imaging based on structured intensity profiles, beam steering will generate a shift in the line structure that, in turn, will lead to an asymmetry in the extracted species image, with a stronger signal on the entrance side (analogous to laser extinction). To investigate whether effects of beam steering can be observed in the data, the excitation line structures are traced across the field-of-view, see Fig. 11, focusing in particular on regions before and after the reaction zone where the temperature gradient is the steepest and thus the impact of beam steering should be the greatest. In the analysis, each modulated line is treated as a single beam and any departure from its optical path should be visually apparent in the recorded data. The

analysis shows, however, no visible traces of beam steering, which is most likely due to the relatively short distance light travels between the two borders of the reaction zone. Measurement issues associated with beam steering may, however, be more pronounced when probing larger combustion systems using FRAME.

5. Summary

In summary, we have, for the first time, applied the FRAME technique for simultaneous multispectral imaging of combustion species. FRAME uses a non-conventional illumination scheme wherein each excitation source is given a unique periodic spatial code (line structure) that can be recognized and isolated by a spatial frequency-sensitive algorithm in the data post-processing. This methodology makes it possible for a single camera to collect several images at the same time. Past methods to achieve simultaneous multispectral imaging in combustion often rely on schemes based on sequential illumination and detection using several intensified, time-gated cameras to avoid signal interference between different signal components. By acquiring all data with a single detector using the FRAME concept, correction procedures to (1) achieve precise pixel-to-pixel overlap and (2) compensate for differences in the collection optics and detector characteristics are no longer needed. Laser sheet-based FRAME imaging does, however, require additional optical access due to the need to illuminate the sample at two angles. Moreover, the current approach to create the intensity modulation yields losses on the excitation side that needs to be addressed experimentally to improve the SNR. Lossless methods to create the periodic line structure using e.g. diffraction optical elements will be investigated in future work.

Since FRAME collects all data during a single acquisition and not in a rapid sequence, fast camera gating becomes less critical. This could potentially allow intensified cameras to be replaced with less expensive, yet more sensitive cameras that also have improved pixel resolution. The robustness of the methodology was investigated in terms of beam steering where no major complications were seen in the current experimental configuration. Furthermore, POD mode analysis was performed on FRAME data of OH and CH_2O with different image resolutions. The results indicate that the spatial resolution of the FRAME data that is achieved here is sufficient for POD mode analysis.

Finally, although FRAME was used here to differentiate between different fluorescence signals, the technique can readily be applied in a variety of alternative optical configurations, e.g. for measurements based on absorption, elastic scattering and polarization.

References

[1] A.C. Eckbreth, Laser diagnostics for combustion temperature and species, Abacus, 1988.

[2] K. Kohse-Hoinghaus, R.S. Barlow, M. Alden, E. Wolfrum, Combustion at the focus: laser diagnostics and control, Proc. Combust. Inst. 30 (2005) 89–123.

[3] Y. Ishino, N. Ohiwa, Three-dimensional computerized tomographic reconstruction of instantaneous distribution of chemiluminescence of a turbulent premixed flame, JSME Int. J. B. Fluid. T. 48 (2005) 34–40.

[4] G. Gilabert, G. Lu, Y. Yan, Three-dimensional tomographic reconstruction of the luminosity distribution of a combustion flame, IEEE Trans. Instrum. Meas. 56 (2007) 1300–1306.

[5] B.R. Halls, D.J. Thul, D. Michaelis, S. Roy, T.R. Meyer, J.R. Gord, Single-shot, volu-
metrically illuminated, three-dimensional, tomographic laser-induced-fluores-
cence imaging in a gaseous free jet, Opt. Express 24 (2016) 10040–10049.

[6] S.A. Skeen, J. Manin, L.M. Pickett, Simultaneous formaldehyde PLIF and high-
-speed schlieren imaging for ignition visualization in high-pressure spray
flames, Proc. Combust. Inst. 35 (2015) 3167–3174.

[7] M.J. Dyer, D.R. Crosley, Two-dimensional imaging of OH laser-induced fluores-
cence in a flame, Opt. Lett. 7 (1982) 382–384.

[8] R. Miles, W. Lempert, 2-dimensional measurement of density, velocity, and
temperature in turbulent high-speed air-flows by UV Rayleigh-scattering, Appl.
Phys. B. 51 (1990) 1–7.

[9] J.H. Frank, S.A. Kaiser, M.B. Long, Reaction-rate, mixture-fraction, and temper-
ature imaging in turbulent methane/air jet flames, Proc. Combust. Inst. 29
(2002) 2687–2694.

[10] C. Brackmann, J. Bood, M. Alden, G. Pengloan, O. Andersson, Quantitative
measurements of species and temperature in a DME-air counterflow diffu-
sion flame using laser diagnostic methods, Combust. Sci. Technol. 178 (2006)
1165–1184.

[11] C. Schulz, B.F. Kock, M. Hofmann, H. Michelsen, S. Will, B. Bougie, R. Suntz,
G. Smallwood, Laser-induced incandescence: recent trends and current ques-
tions, Appl. Phys. B: Lasers Opt. 83 (2006) 333–354.

[12] R.J. Adrian, Twenty years of particle image velocimetry, Exp. Fluids 39 (2005)
159–169.

[13] Z.S. Li, B. Li, Z.W. Sun, X.S. Bai, M. Alden, Turbulence and combustion interac-
tion: High resolution local flame front structure visualization using simultane-
ous single-shot PLIF imaging of CH, OH, and CH2O in a piloted premixed jet
flame, Combust. Flame 157 (2010) 1087–1096.

[14] J. Kiefer, Z.S. Li, J. Zetterberg, X.S. Bai, M. Alden, Investigation of local flame
structures and statistics in partially premixed turbulent jet flames using si-
multaneous single-shot CH and OH planar laser-induced fluorescence imaging,
Combust. Flame 154 (2008) 802–818.

[15] M. Roder, T. Dreier, C. Schulz, Simultaneous measurement of localized heat-re-
lease with OH/CH2O-LIF imaging and spatially integrated OH* chemilumines-
cence in turbulent swirl flames, Proc. Combust. Inst. 34 (2013) 3549–3556.

[16] R.L. Gordon, A.R. Masri, E. Mastorakos, Simultaneous Rayleigh temperature,
OH- and CH2O-LIF imaging of methane jets in a vitiated coflow, Combust.
Flame 155 (2008) 181–195.

[17] J. Sjoholm, J. Rosell, B. Li, M. Richter, Z.S. Li, X.S. Bai, M. Alden, Simultaneous
visualization of OH, CH, CH2O and toluene PLIF in a methane jet flame with
varying degrees of turbulence, Proc. Combust. Inst. 34 (2013) 1475–1482.

[18] S. Bockle, J. Kazenwadel, T. Kunzelmann, C. Schulz, Laser-diagnostic multi-
-species imaging in strongly swirling natural gas flames, Appl. Phys. B: Lasers
Opt. 71 (2000) 741–746.

[19] S. Bockle, J. Kazenwadel, T. Kunzelmann, D.I. Shin, C. Schulz, J. Wolfrum, Simul-
taneous single-shot laser-based imaging of formaldehyde, OH, and temperature
in turbulent flames, Proc. Combust. Inst. 28 (2000) 279–286.

[20] P.R. Medwell, P.A.M. Kalt, B.B. Dally, Simultaneous imaging of OH, formalde-
hyde, and temperature of turbulent nonpremixed jet flames in a heated and
diluted coflow, Combust. Flame 148 (2007) 48–61.

[21] M. Tanahashi, S. Murakami, G.M. Choi, Y. Fukuchi, T. Miyauchi, Simultaneous
CH-OHPLIF and stereoscopic PIV measurements of turbulent premixed flames,
Proc. Combust. Inst. 30 (2005) 1665–1672.

[22] B. Zhou, C. Brackmann, Z.S. Li, M. Alden, X.S. Bai, Simultaneous multi-species
and temperature visualization of premixed flames in the distributed reaction
zone regime, Proc. Combust. Inst. 35 (2015) 1409–1416.

[23] E. Kristensson, Z. Li, E. Berrocal, M. Richter, M. Alden, Instantaneous 3D imag-
ing of flame species using coded laser illumination, Proc. Combust. Inst. 36
(2017) 4585–4591.

[24] A. Ehn, J. Bood, Z. Li, E. Berrocal, M. Alden, E. Kristensson, FRAME: femtosecond
videography for atomic and molecular dynamics, Light: Sci. Appl. 6 (2017) 1–7,
doi:10.1038/lsa.2017.45.

[25] K. Dorozynska, E. Kristensson, Implementation of a multiplexed structured il-
lumination method to achieve snapshot multispectral imaging, Opt. Express 25
(2017) 17211–17226.

[26] E. Kristensson, E. Berrocal, M. Alden, Two-pulse structured illumination imag-
ing, Opt. Lett. 39 (2014) 2584–2587.

[27] E. Berrocal, E. Kristensson, M. Richter, M. Linne, M. Alden, Application of struc-
tured illumination for multiple scattering suppression in planar laser imaging
of dense sprays, Opt. Express 16 (2008) 17870–17881.

[28] E. Kristensson, E. Berrocal, M. Richter, S.G. Pettersson, M. Alden, High-speed
structured planar laser illumination for contrast improvement of two-phase
flow images, Opt. Lett. 33 (2008) 2752–2754.

[29] E. Kristensson, J. Bood, M. Alden, E. Nordstrom, J.J. Zhu, S. Huldt, P.E. Bengtsson,
H. Nilsson, E. Berrocal, A. Ehn, Stray light suppression in spectroscopy using
periodic shadowing, Opt. Express 22 (2014) 7711–7721.

[30] E. Kristensson, A. Ehn, E. Berrocal, High dynamic spectroscopy using a digital
micromirror device and periodic shadowing, Opt. Express 25 (2017) 212–222.

[31] E. Kristensson, A. Ehn, J. Bood, M. Alden, Advancements in Rayleigh scatter-
ing thermometry by means of structured illumination, Proc. Combust. Inst. 35
(2015) 3689–3696.

[32] J. Sjöholm, J. Rosell, B. Li, M. Richter, Z. Li, X.-S. Bai, M. Aldén, Simultaneous
visualization of OH, CH, CH2O and toluene PLIF in a methane jet flame with
varying degrees of turbulence, Proc. Combust. Inst. 34 (2013) 1475–1482.

[33] P.H. Paul, H.N. Najm, Planar laser-induced fluorescence imaging of flame heat
release rate, 27th Symposium (International) on Combustion 27 (1) (1998)
43–50.

[34] B. Zhou, C. Brackmann, Q. Li, Z.K. Wang, P. Petersson, Z.S. Li, M. Alden, X.S. Bai,
Distributed reactions in highly turbulent premixed methane/air flames Part I.
Flame structure characterization, Combust. Flame 162 (2015) 2937–2953.

[35] A.A. Subash, R. Whiddon, R. Collin, M. Aldén, A. Kundu, J. Klingmann, Flame in-
vestigation of a gas turbine central pilot body burner at atmospheric pressure
conditions using OH PLIF and high-speed flame chemiluminescence imaging,
ASME 2015 Gas Turbine India Conference, ASME (2015).

[36] P. Iudiciani, C. Duwig, S.M. Husseini, R.Z. Szasz, L. Fuchs, E.J. Gutmark, Proper
orthogonal decomposition for experimental investigation of flame instabilities,
AIAA J. 50 (2012) 1843–1854.

[37] G. Berkooz, P. Holmes, J.L. Lumley, The proper orthogonal decomposition in the
analysis of turbulent flows, Annu. Rev. Fluid Mech. 25 (1993) 539–575.

[38] K. Taira, S.L. Brunton, S.T.M. Dawson, C.W. Rowley, T. Colonius, B.J. McKeon,
O.T. Schmidt, S. Gordeyev, V. Theofilis, L.S. Ukeiley, Modal analysis of fluid
flows: an overview, AIAA J. (2017) arXiv:1702.01453 [physics.flu-dyn], doi:10.
2514/1.J056060.

[39] C. Brackmann, J. Nygren, X. Bai, Z.S. Li, H. Bladh, B. Axelsson, I. Denbratt,
L. Koopmans, P.E. Bengtsson, M. Alden, Laser-induced fluorescence of formalde-
hyde in combustion using third harmonic Nd:YAG laser excitation, Spec-
trochim. Acta A 59 (2003) 3347–3356.

[40] M.C. Thurber, F. Grisch, B.J. Kirby, M. Votsmeier, R.K. Hanson, Measurements
and modeling of acetone laser-induced fluorescence with implications for tem-
perature-imaging diagnostics, Appl. Opt. 37 (1998) 4963–4978.

[41] C. Schulz, V. Sick, Tracer-LIF diagnostics: quantitative measurement of fuel
concentration, temperature and fuel/air ratio in practical combustion systems,
Prog. Energy Combust. 31 (2005) 75–121.

[42] N.B. Jiang, R.A. Patton, W.R. Lempert, J.A. Sutton, Development of high-repeti-
tion rate CH PLIF imaging in turbulent non-premixed flames, Proc. Combust.
Inst. 33 (2011) 767–774.

[43] J.A. Sutton, J.F. Driscoll, Optimization of CH fluorescence diagnostics in flames:
range of applicability and improvements with hydrogen addition, Appl. Opt. 42
(2003) 2819–2828.

[44] C.M. Vagelopoulos, J.H. Frank, An experimental and numerical study on the ad-
equacy of CH as a flame marker in premixed methane flames, Proc. Combust.
Inst. 30 (2005) 241–249.

[45] P.A. Bonczyk, J.A. Shirley, Measurement of CH and CN concentration in flames
by laser-induced saturated fluorescence, Combust. Flame 34 (1979) 253–264.

[46] C. Chan, J.W. Daily, Measurement of temperature in flames using laser-induced
fluorescence spectroscopy of OH, Appl. Opt. 19 (1980) 1963–1968.

[47] M. Alden, H. Edner, G. Holmstedt, S. Svanberg, T. Hogberg, Single-pulse
laser-induced OH fluorescence in an atmospheric flame, spatially resolved with
a diode-array detector, Appl. Opt. 21 (1982) 1236–1240.

[48] W. Koban, J.D. Koch, R.K. Hanson, C. Schulz, Oxygen quenching of toluene
fluorescence at elevated temperatures, Appl. Phys. B: Lasers Opt. 80 (2005)
777–784.

[49] M.G. Allen, K.R. Mcmanus, D.M. Sonnenfroh, P.H. Paul, Planar laser-induced-flu-
orescence imaging measurements of OH and hydrocarbon fuel fragments in
high-pressure spray-flame combustion, Appl. Opt. 34 (1995) 6287–6300.

[50] R. Suntz, H. Becker, P. Monkhouse, J. Wolfrum, Two-dimensional visualization
of the flame front in an internal-combustion engine by laser-induced fluores-
cence of OH radicals, Appl. Phys. B. 47 (1988) 287–293.

[51] A. Gersho, R.M. Gray, Vector quantization and data compression, Kluwer, 1991.